

Numerical and analytical study of undular bores governed by the full water wave equations and bidirectional Whitham–Boussinesq equations

Cite as: Phys. Fluids **33**, 067105 (2021); <https://doi.org/10.1063/5.0050067>

Submitted: 11 March 2021 . Accepted: 13 May 2021 . Published Online: 03 June 2021

 Rosa María Vargas-Magaña,  T. R. Marchant, and  Noel F. Smyth



View Online



Export Citation



CrossMark

Physics of Fluids

SPECIAL TOPIC: Tribute to
Frank M. White on his 88th Anniversary

SUBMIT TODAY!



Numerical and analytical study of undular bores governed by the full water wave equations and bidirectional Whitham–Boussinesq equations

Cite as: Phys. Fluids **33**, 067105 (2021); doi: 10.1063/5.0050067

Submitted: 11 March 2021 · Accepted: 13 May 2021 ·

Published Online: 3 June 2021



View Online



Export Citation



CrossMark

Rosa María Vargas-Magaña,¹  T. R. Marchant,^{2,3,a)}  and Noel F. Smyth^{1,2} 

AFFILIATIONS

¹School of Mathematics, University of Edinburgh, Edinburgh EH9 3FD, Scotland, United Kingdom

²School of Mathematics and Applied Statistics, University of Wollongong, Northfields Avenue, Wollongong, NSW 2522, Australia

³Australian Mathematical Sciences Institute, University of Melbourne, Melbourne, Victoria 3052, Australia

^{a)} Author to whom correspondence should be addressed: tim_marchant@uow.edu.au

ABSTRACT

Undular bores, also termed dispersive shock waves, generated by an initial discontinuity in height as governed by two forms of the Boussinesq system of weakly nonlinear shallow water wave theory, the standard formulation and a Hamiltonian formulation, two related Whitham–Boussinesq equations, and the full water wave equations for gravity surface waves are studied and compared. It is found that the Whitham–Boussinesq systems give solutions in excellent agreement with numerical solutions of the full water wave equations for the positions of the leading and trailing edges of the bore up until the onset on modulational instability. The Whitham–Boussinesq systems, which are far simpler than the full water wave equations, can then be used to accurately model surface water wave undular bores. Finally, comparisons with numerical solutions of the full water wave equations show that the Whitham–Boussinesq systems give a slightly lower threshold for the onset of modulational instability in terms of the height of the initial step generating the undular bore.

Published under an exclusive license by AIP Publishing. <https://doi.org/10.1063/5.0050067>

I. INTRODUCTION

Dispersive shock waves (DSW), also termed undular bores in fluid mechanics applications, are a generic type of wave phenomenon arising as solutions of nonlinear dispersive wave equations. DSWs are formed due to the dispersive regularization of a wave breaking singularity or an initial jump discontinuity, as opposed to the viscous shocks of compressible flow in which viscosity smooths the shock.¹ In their generic form, they are a modulated wavetrain, consisting of solitary waves at one edge and linear dispersive waves at the opposite edge, which links two disparate flow states, thus displaying a range of nonlinearities within a single coherent structure.² In addition to their theoretical interest as a generic nonlinear wave form, DSWs are readily observable in a wide range of applications, examples including meteorology,^{3–5} oceanography,^{6–10} water waves,^{7,8,11} plasmas,¹² geophysics,^{13–16} nonlinear optics,^{17–26} elasticity,²⁷ Bose–Einstein condensates,²⁸ magnetic films,²⁹ and Fermionic fluids;³⁰ see Ref. 2 for a summary of these applications.

The unsteady, multiscale dynamics of DSWs, which exhibit diverging leading and trailing edges, have far reaching physical and mathematical implications, among which are the inapplicability of the classical Rankine–Hugoniot shock conditions and the inseparability of

the macroscopic DSW dynamics from its microscopic nonlinear oscillatory structure.² The mathematical description of DSWs involves a synthesis of methods from hyperbolic quasi-linear systems, asymptotic theory and solitary wave theory. One of the principal tools used to analyze DSWs is Whitham modulation theory.^{1,31,32} Within this theory, DSWs are typically described as simple wave solutions of the Whitham modulation equations when the underlying modulated wavetrain is stable, so that the modulation system is hyperbolic. The first such solution was constructed by Gurevich and Pitaevskii for the KdV equation,³³ based on the Whitham modulation equations for the KdV equation.^{1,32}

The derivation of a DSW solution from the Whitham modulation equations for a nonlinear dispersive wave equation requires that these be set in Riemann invariant form, which is only guaranteed if the underlying equation is integrable³⁴ or that they form a second-order system.¹ These restrictions rule out finding DSW solutions of many nonlinear dispersive equations arising in applications. In a major advance, it was realized that Whitham modulation equations have a degenerate form in their solitary wave and linear wave limits. A result of this is that the solitary wave and linear wave edges can be

determined for general nonlinear dispersive wave equations.^{2,35} This method for determining the edges of a DSW is termed the dispersive shock fitting method and determines these DSW edges for DSWs of “KdV-type.” The basic constraints for the existing analytical theory for DSWs identified in the review² are (i) one spatial dimension, (ii) constant coefficients for the nonlinear and dispersive terms, (iii) the existence of steady traveling wave solutions, and solitary wave solutions, in particular, (iv) convexity of the linear dispersion relation, (v) strict hyperbolicity and genuine nonlinearity of the long wave (dispersionless) limit, and (vi) strict hyperbolicity and genuine nonlinearity of the associated nonlinear modulation (Whitham) system.

This work is concerned with the classical topic of surface water wave DSWs. As we are concerned with DSWs as a surface water wave, the term undular bore will be used for this type of DSW to conform with the fluid mechanics terminology. Undular bores governed by two versions of the Boussinesq system, the standard version,¹ termed System A, and one derived from the Hamiltonian form of the water wave equations,^{36–38} termed System B, and their related Whitham–Boussinesq equations,^{39,40,42,43} will be studied. These undular bore solutions will be found using the dispersive shock fitting method and will be compared with solutions of the full water wave equations. Weakly nonlinear, long wave equations, such as, the Korteweg–de Vries (KdV) and Boussinesq equations,¹ which are approximations to the full water wave equations, do not exhibit short wave effects, such as, breaking and peaking which are exhibited by solutions of the full water wave equations. To explore short wave effects in the context of weakly nonlinear dispersive wave equations, Whitham proposed replacing the third order dispersion of the KdV equation with full water wave dispersion, resulting what is now termed as the Whitham equation

$$\frac{\partial u}{\partial t} - \frac{\partial u}{\partial x} + 6u \frac{\partial u}{\partial x} + \int_{-\infty}^{\infty} K(x - \xi) u_{\xi}(\xi, t) d\xi = 0, \tag{1}$$

$$K = F^{-1} \left\{ \sqrt{\frac{\tanh k}{k}} \right\},$$

where F^{-1} denotes the inverse Fourier transform.^{1,44} Expanding $\tanh k$ in a Taylor series to $O(k^3)$ results in the KdV equation. An analysis of this Whitham equation, and related equations, shows that their solutions exhibit the short wave effects of breaking and peaking, limiting solutions of largest height (reminiscent of the cusped Stokes water wave of greatest height).^{1,45–50} While these unidirectional models with nonlocal terms, such as, (1), were proposed in order to study particular effects and were not derived directly from the water wave equations, recently Craig *et al.*⁵¹ reconsidered the problem of long water waves using expansions of the nonlocal operators arising in the Hamiltonian formulation of the water wave equations, which are valid for arbitrary bottom topography. The end result is a Hamiltonian formulation in terms of pseudodifferential operators which can be calculated recursively in terms of the shape of the wave and the depth variation. It was subsequently shown that bidirectional analogues of the Whitham equation can be derived from the Hamiltonian formulation of the water wave equations.^{39,40,52} Two bidirectional Whitham equation systems will be studied in this paper. One is derived following Whitham’s heuristic derivation of the original Whitham equation (1) using a combination of the full dispersion relation of water waves and the nonlinear convection term of the shallow water equations, introduced as the

“full-dispersion shallow water equations.”^{41,42} The other is derived using the Hamiltonian formulation of the water wave equations,⁵¹ which has the benefit of being a valid asymptotic approximation of the full water wave equations.

In addition, solutions of the Whitham equation (1) and bidirectional analogues of the Whitham equation were found to be in as good, or even better, agreement with solutions of the full water wave equations as compared with the KdV, the Benjamin–Bona–Mahony equation, the Serre equations and the shallow water equations.^{39,52,53} Whitham equations have also been found to give solutions in better agreement with experimental results for shallow water waves than the KdV equation or Serre equations.⁴³ Two of the bidirectional Whitham systems whose solutions were compared with experimental results⁴³ are also used in the present work and are referred to as Systems C and D. System D is derived from the Hamiltonian formulation of the water wave equations, while System C is proposed^{41,42} in the same manner as Whitham did for the original Whitham equation.¹ Previous work has shown that the undular bore solution of the Whitham equation (1) differs substantially from the KdV undular bore as the height of the initial step which generates the bore grows and that it exhibits short wave Benjamin–Feir instability for a high enough initial step.⁶⁵

The organization of the paper is as follows. In Sec. II, we formulate the water wave problem using Dirichlet–Neumann operators based on the Hamiltonian formulation of the water wave equations and cite and derive four weakly nonlinear systems, including the standard Boussinesq system¹ and a Boussinesq system derived from the Hamiltonian formulation of the water wave equations,^{36–38} referred to as Systems A and B, and Whitham–Boussinesq systems derived from these, referred to as Systems C and D. In Sec. III, we derive the dispersion relations for the four Boussinesq systems studied and the dispersionless limits associated with each of these weakly nonlinear systems. In Sec. IV, we use the dispersive shock fitting method^{2,35} to find the solutions for the leading and trailing edges of a bore as governed by each of these four Boussinesq systems. Finally, in Sec. V we compare results of the Boussinesq systems with full numerical solutions of the water wave equations. The role of short wave effects on the development of Benjamin–Feir instability in the bore is made clear, with particular reference to how this instability evolves as the bore amplitude grows.^{1,54} The inclusion of short wave effects via the full water wave dispersion relation in the Whitham–Boussinesq systems is needed for a Boussinesq system to predict this instability.

II. WHITHAM–BOUSSINESQ EQUATIONS

Let us consider two dimensional (depth and horizontal direction) gravity waves on the surface of an inviscid, incompressible fluid of undisturbed depth h_0 bounded below by an impermeable horizontal bottom. We take the y direction to be opposite to the direction of gravity and x horizontal. The water wave equations¹ in terms of the velocity potential φ and the surface displacement $\eta(x, y)$ are

$$\nabla^2 \varphi = 0, \tag{2}$$

within the fluid, together with the surface conditions

$$\eta_t + \varphi_x \eta_x = \varphi_y, \tag{3}$$

$$\varphi_t + \frac{1}{2} |\nabla \varphi|^2 + g\eta = 0, \tag{4}$$

at $y = \eta(x)$ and the bottom boundary condition

$$\nabla\varphi \cdot N(\beta) = 0, \tag{5}$$

at $y = -h_0 + \beta(x)$, where $N(\beta)$ is the exterior unit normal on the rigid boundary. It was shown by Zakharov³⁸ that these water wave equations can be stated as a Hamiltonian system with infinitely many degrees of freedom in terms of the wave amplitude $\eta(x, t)$ and surface hydrodynamic potential $\xi(x, t) = \varphi(x, \eta(x, t), t)$.^{36,37} This Hamiltonian formulation is

$$\partial_t \begin{pmatrix} \eta \\ \xi \end{pmatrix} = \begin{pmatrix} 0 & I \\ -I & 0 \end{pmatrix} \begin{pmatrix} \frac{\delta H}{\delta \eta} \\ \frac{\delta H}{\delta \xi} \end{pmatrix}, \tag{6}$$

where the Hamiltonian is expressed explicitly in terms of η and ξ as

$$H = \frac{1}{2} \int_{\mathbb{R}} [\xi G(\beta, \eta) \xi + g\eta^2] dx, \tag{7}$$

see Ref. 55. The Hamiltonian formulation was originally developed for a fluid of varying depth, but here we consider a fixed depth, $\beta(x) \equiv 0$; in this case, let us now introduce the *Dirichlet–Neumann operator* $G(\eta)$, which is defined as follows. Fix η and ξ , let φ be the (unique) solution of the boundary value problem,

$$\begin{aligned} \nabla^2 \varphi(x, y) &= 0 \quad \forall (x, y) \in \mathcal{D}_t(\eta) : \\ &= \{(x, y) : x \in \mathbb{R}, -h_0 < y < \eta(x, t)\}, \end{aligned} \tag{8}$$

$$\varphi(x, \eta(x)) = \xi(x) \quad \forall x \in \mathbb{R}, \tag{9}$$

$$\frac{\partial \varphi}{\partial n}(x, -h_0) = 0 \quad \forall x \in \mathbb{R}, \tag{10}$$

in the two-dimensional (time-dependent) simply connected domain $\mathcal{D}_t(\eta)$ together with the appropriate periodic or asymptotic conditions on φ , and we define the Dirichlet–Neumann operator $G(\eta)$ by

$$(G(\eta))[\xi(x)] = [1 + (\partial_x \eta(x))^2]^{\frac{1}{2}} \nabla \varphi(x, \eta(x)) \cdot N(\eta(x)), \tag{11}$$

where

$$N(\eta(x)) = [1 + (\partial_x \eta(x))^2]^{-\frac{1}{2}} (-\partial_x \eta(x), 1) \quad x \in \mathbb{R}, \tag{12}$$

is the exterior unit normal at the free surface. The Dirichlet–Neumann operator $G(\eta)$ is a linear operator on ξ . However, it is nonlinear with explicitly nonlocal behavior in the two functions $\beta(x)$ and $\eta(x)$, which give the lower and upper boundaries of the fluid domain. This operator maps Dirichlet data for harmonic functions to Neumann data at the free surface and is symmetric with respect to the usual L^2 inner product. Note that definition (11) for the Dirichlet–Neumann operator is given in abstract terms as there is no explicit expression for this operator for a general fluid domain. In order to obtain $[G(\eta)][\xi(x)]$, given the function ξ , the surface hydrodynamic potential at time t , we need to solve the elliptic problem described by (8)–(10) and then solve a nonlocal equation to obtain the normal derivative of the hydrodynamic potential. This is then evaluated at the free surface, thus obtaining the mapping $[G(\eta)][\xi(x)]$.

Craig *et al.*⁵¹ give an expansion of the operator $G(\eta)$ as

$$G(\eta) = G_0(\eta) + G_1(\eta) + G_2(\eta) + \dots, \tag{13}$$

where the G_j are homogeneous of degree j in η . The explicit expressions for the first terms in this expansion are

$$G_0(\eta) = D \tanh(h_0 D), \tag{14}$$

$$G_1(\eta) = D\eta D - G_0\eta G_0, \tag{15}$$

$$G_2(\eta) = \frac{1}{2} (G_0 D \eta^2 D - D^2 \eta^2 G_0 - 2G_0 \eta G_1), \tag{16}$$

where $D = -i\partial_x$ and $G_0 = G_0(\eta)$. Here, we are using the notation

$$[a(f(x)D^m)\xi](x) = \int_{\mathbb{R}} a(f(x)k^m) \hat{\xi}(k) e^{ikx} dk, \tag{17}$$

where a and f are real functions and

$$\hat{\xi}(k) = \frac{1}{2\pi} \int_{\mathbb{R}} \xi(x) e^{-ikx} dx \tag{18}$$

is the Fourier transform of the real function ξ . At higher order, the G_j , $j > 2$, are similarly obtained from G_0 using a recursion relation.⁵¹

The Hamiltonian evolution equations (6) and (7) can be set in terms of the velocity potential at the surface $\xi = \varphi[x, \eta(x)]$ and the surface displacement $\eta(x, y)$ as

$$\eta_t = G(\beta, \eta)\xi, \tag{19}$$

$$\xi_t = -\frac{1}{2(1 + \eta_x^2)} \left[\xi_x^2 - (G(\beta, \eta)\xi)^2 + 2\eta_x \xi_x G(\beta, \eta)\xi \right] - g\eta. \tag{20}$$

Let us now consider the water wave equations in the shallow water limit, that is, a typical wavelength is much greater than the fluid depth h_0 . Let us take a typical wavelength to be l and a typical wave amplitude to be a . We then define two nondimensional parameters $\alpha = a/h_0$ and $\delta = (h_0/l)^2$. The Hamiltonian (7) takes the form of a polynomial in η of pseudodifferential operators acting on the variable ξ . To obtain the Boussinesq–Whitham approximation, we Taylor expand all the Fourier multipliers in G , such as, $\tanh(h_0 D)$, in powers of the derivative $h_0 D$. However, to keep the full linear dispersion relation we follow Whitham^{1,44} and use the exact expression for the constant depth quadratic part $\frac{1}{2} \int_{\mathbb{R}} \xi D \tanh(h_0 D) dx$ and apply the expansion to powers of derivatives in all remaining terms of H . Finally, we use the usual Boussinesq scaling $\alpha = \delta$ to approximate the remaining terms. To this end, we scale the wavelength in the shallow water form $l = h_0/\sqrt{\delta}$ and take $\varepsilon = \alpha = \delta \ll 1$. Finally, let us now use nondimensional variables so that $h_0 = 1$ and $g = 1$. We then have $H = H_0 + O(\varepsilon^2)$, with H_0 the Whitham–Boussinesq Hamiltonian given by

$$H_0 = \frac{1}{2} \int_{\mathbb{R}} (\xi D \tanh(D)\xi + \eta(\partial_x \xi)^2 + \eta^2) dx. \tag{21}$$

Hamilton’s equation (6) associated with this Whitham–Boussinesq Hamiltonian (21) gives the following system, on setting $u = \xi_x$,

$$\eta_t = -\partial_x \left(\left[\frac{\tanh D}{D} \right] u \right) - (\eta u)_x, \tag{22}$$

$$u_t = -\eta_x - uu_x. \tag{23}$$

We shall term this system the Whitham–Boussinesq–Hamiltonian system. To understand the relationship between this system and

standard Boussinesq systems, we expand the differential operator $\tanh D$ in the Hamiltonian (21) in a Taylor series to second order, resulting in

$$H_{00} = \frac{1}{2} \int_{\mathbb{R}} \xi \left((D)^2 - \frac{1}{3} (D)^4 \right) \xi + \eta (\partial_x \xi)^2 + \eta^2 dx. \quad (24)$$

Computing the variational derivatives of this functional given by (6), we obtain the system

$$\eta_t = -\xi_{xx} - \frac{1}{3} \xi_{xxxx} - (\eta \xi_x)_x, \quad (25)$$

$$\xi_t = -\eta - \frac{1}{2} \xi_x^2. \quad (26)$$

Now, if we introduce the horizontal velocity $u = \xi_x$ and differentiate (26) with respect to x , we obtain the system (28) below. This system is a variation of the standard Boussinesq system from shallow water theory.¹

A. Weakly nonlinear systems

The undular bore solutions of the Whitham–Boussinesq–Hamiltonian systems and the Boussinesq systems will be compared with numerical bore solutions of the full water wave equations (2)–(5). To obtain an understanding of the role of short wave effects and the accuracy of the various Boussinesq systems, the undular bore solution of the standard Boussinesq system¹ and its related Whitham–Boussinesq system will also be obtained. We shall then obtain the undular bore solutions of the following four Boussinesq systems.

System A The standard Boussinesq system¹

$$\begin{aligned} \eta_t &= -u_x - (\eta u)_x, \\ u_t &= -uu_x - \eta_x - \frac{1}{3} \eta_{xxx}. \end{aligned} \quad (27)$$

System B The Boussinesq system derived from the Hamiltonian (24), termed the Boussinesq–Hamiltonian system⁵¹

$$\begin{aligned} \eta_t &= -u_x - \frac{1}{3} u_{xxx} - (\eta u)_x, \\ u_t &= -\eta_x - uu_x. \end{aligned} \quad (28)$$

System C This Whitham–Boussinesq system has been derived from a combination of the full dispersion relation for water waves and the convective term of the nonlinear shallow water equations. The system has been termed the “full-dispersion shallow water equations”^{41,42} and is

$$\begin{aligned} \eta_t &= -u_x - (\eta u)_x, \\ u_t &= -uu_x - \partial_x \left(\left[\frac{\tanh D}{D} \right] \eta \right). \end{aligned} \quad (29)$$

System D This Whitham–Boussinesq–Hamiltonian system has been derived from the Hamiltonian formulation of the water wave equations (21),³⁹

$$\begin{aligned} \eta_t &= -\partial_x \left(\left[\frac{\tanh D}{D} \right] u \right) - (\eta u)_x, \\ u_t &= -\eta_x - uu_x. \end{aligned} \quad (30)$$

The initial condition used to generate the undular bore is the step initial condition in wave height,

$$\eta(x, 0) = \begin{cases} \eta_- & x < 0, \\ \eta_+ & x > 0. \end{cases} \quad (31)$$

The initial velocity is chosen to be $u(x, 0) = 0$ for simplicity. The analysis of the present work could be easily extended to include a jump in the initial velocity.

The undular bore solutions of these four Boussinesq systems have a common general structure. A typical solution is shown in Fig. 1 for the Whitham–Boussinesq–Hamiltonian system (30), System D, for the initial condition (31) with $\eta_+ = 0$ and $\eta_- = 0.2$. The initial condition breaks up into a backward propagating expansion wave and a forward propagating undular bore, connected by an intermediate shelf of height η_b , as typical for bidirectional nonlinear dispersive wave equations whose periodic wave solution is modulationally stable.² The undular bore is a slowly varying modulated wavetrain whose wavenumber $k \rightarrow 0$ at the leading edge, so that the leading edge consists of solitary waves. At the trailing edge, the amplitude of the wavetrain $a \rightarrow 0$, so that the trailing edge consists of linear dispersive waves. The solution for the backward propagating expansion wave is given by a simple wave solution of the non-dispersive limit of the relevant Boussinesq system.² This expansion wave solution is not the focus of the present work, as the undular bore is the focus, and comparisons between the expansion wave solution of the Boussinesq systems and solutions of the full water wave equations will not be given here. The solution shown in the figure is the dispersive equivalent of the solution of the shock tube problem of compressible flow,¹ with the undular bore replacing the gasdynamic shock wave. The solution in Fig. 1 is shown at the time $t = 200$ so that the separation between the (backward propagating) expansion wave and the (forward propagating) undular bore is not so great that the details of the bore would not be visible in the figure.

As discussed in the Introduction, to obtain the full undular bore solution of a nonlinear, dispersive wave equation, the Whitham modulation equations for this equation need to be known. As these modulation equations are not known for the four Boussinesq systems studied in this work, the leading and trailing edges of the undular bore

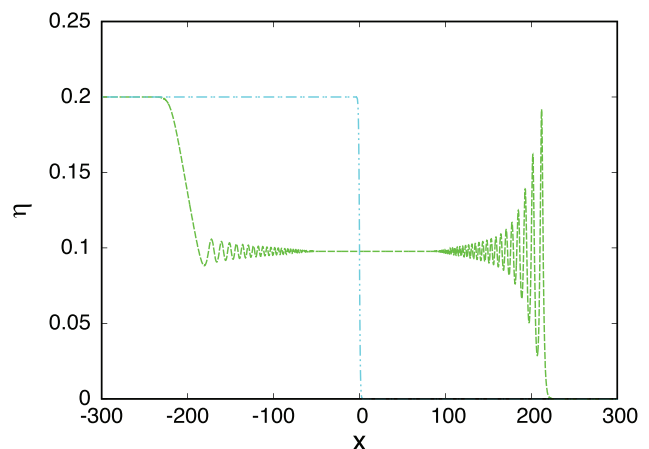


FIG. 1. Typical solution of the Whitham–Boussinesq–Hamiltonian system (30), System D, for the surface elevation η : green (dashed) line. Initial condition (31): blue (dotted-dotted-dashed) line. Here, $\eta_+ = 0$, $\eta_- = 0.2$, and $t = 200$.

solutions of the four Boussinesq systems will be found using the dispersive shock fitting method.^{2,35} All that is required for the application of this method is the linear dispersion relation for the relevant equation. The dispersive shock fitting method then determines the velocities of the leading and trailing edges of the undular bore. To determine the amplitude of the leading edge, the amplitude-velocity relation for the solitary wave solution needs to be determined. This can be found for the Boussinesq systems (27) and (28), but not for the Whitham-Boussinesq equations. The amplitude-velocity relations for the solitary wave solutions of Systems A and B, the standard Boussinesq systems, will now be found.

System A Standard Boussinesq system

Let us seek the solitary wave solution of the standard Boussinesq system¹ (27), system A, with $u = u(\theta)$ and $\eta = \eta(\theta)$, where $\theta = x - Vt$. Substituting into the Boussinesq system, eliminating between the equations and integrating once gives

$$-V^2\eta - \frac{V^2}{1+\eta} + \eta^2 + \frac{1}{3}\eta'^2 = -V^2. \tag{32}$$

At the solitary wave maximum, $\eta' = 0$ and $\eta = a$, so that the amplitude-velocity relation for the solitary wave is

$$V = \sqrt{1+a}. \tag{33}$$

System B Boussinesq-Hamiltonian system⁵¹

In a similar manner, we can determine the amplitude-velocity relation for the Boussinesq-Hamiltonian system (28). We again seek solutions of the forms $u = u(\theta)$ and $\eta = \eta(\theta)$. Substituting these into the Boussinesq-Hamiltonian system and integrating once gives

$$\frac{1}{3}u'^2 + (1 - V^2)u^2 + Vu^3 - \frac{1}{4}u^4 = 0. \tag{34}$$

At the solitary wave maximum $u' = 0$, so that the amplitude-velocity relation is

$$V = 1 + \frac{1}{2}a, \tag{35}$$

for a right traveling solitary wave. For small amplitude a , this is asymptotically the same as that for the standard Boussinesq system (33).

III. UNDULAR BORE SOLUTIONS

All four Boussinesq systems (27)–(30) have the same non-dispersive limit,

$$\eta_t + u_x + (\eta u)_x = 0, \tag{36}$$

$$u_t + \eta_x + uu_x = 0. \tag{37}$$

This hyperbolic system can be set in the Riemann invariant form,

$$C_+ : u + 2\sqrt{1+\eta} = R_+ \quad \text{on} \quad \frac{dx}{dt} = u + \sqrt{1+\eta} = V_+, \tag{38}$$

$$C_- : u - 2\sqrt{1+\eta} = R_- \quad \text{on} \quad \frac{dx}{dt} = u - \sqrt{1+\eta} = V_-. \tag{39}$$

The backward propagating expansion wave seen in Fig. 1 forms on the characteristic C_- with the solution constant on the characteristics C_+ . We then have that the Riemann invariant R_+ is

$$u + 2\sqrt{1+\eta} = 2\sqrt{1+\eta_-}, \tag{40}$$

on using the initial condition (31). We then have that the expansion wave solution is

$$\eta = \begin{cases} \eta_-, & -\sqrt{1+\eta_-} < \frac{x}{t}, \\ \frac{1}{9} \left[2\sqrt{1+\eta_-} - \frac{x}{t} \right]^2 - 1, & -\sqrt{1+\eta_-} \leq \frac{x}{t} \leq 2\sqrt{1+\eta_-} - 3\sqrt{1+\eta_i}, \\ \eta_i, & 2\sqrt{1+\eta_-} - 3\sqrt{1+\eta_i} < \frac{x}{t} \leq s_-, \end{cases} \tag{41}$$

with $u = 2\sqrt{1+\eta_-} - 2\sqrt{1+\eta}$. Here, s_- is the velocity of the trailing edge of the undular bore.

The non-dispersive equations in Riemann invariant form (38) and (39) can also be used to determine the intermediate level η_i . The Riemann invariant on the characteristic C_- is conserved through the undular bore.^{2,35} Hence

$$u - 2\sqrt{1+\eta} = -2\sqrt{1+\eta_i}. \tag{42}$$

Using the Riemann invariant on C_+ (40) then gives the intermediate level and the velocity on the intermediate level u_i as

$$\begin{aligned} \sqrt{1+\eta_i} &= \frac{1}{2} \left[\sqrt{1+\eta_+} + \sqrt{1+\eta_-} \right], \\ u_i &= \sqrt{1+\eta_-} - \sqrt{1+\eta_+}. \end{aligned} \tag{43}$$

This completes the solution outside of the undular bore region for all four Boussinesq systems.

A. System A: Standard Boussinesq system

Let us now find the leading and trailing edges of the undular bore solution of the standard Boussinesq system (27) using the dispersive shock fitting method.^{2,35} The basis of the dispersive shock fitting method is the linear dispersion relation for the governing equation. We seek this dispersion relation using linearizations about mean levels $\bar{\eta}$ in η and \bar{u} in u ,

$$\eta = \bar{\eta} + Ae^{i(kx-\omega t)}, \quad u = \bar{u} + Be^{i(kx-\omega t)}, \tag{44}$$

where $|A| \ll |\bar{\eta}|$ and $|B| \ll |\bar{u}|$. Substituting these into the standard Boussinesq system (27) gives, after some algebra, the dispersion relation

$$\omega^{System A}(\bar{\eta}, k) = \bar{u}k + k\sqrt{(1+\bar{\eta})\left(1 - \frac{1}{3}k^2\right)}. \tag{45}$$

The basis of the dispersive shock fitting method is that the Whitham modulation equations are degenerate in the linear wave and solitary wave limits. In the linear wave limit, this results in a compatibility condition, which is the ordinary differential equation,

$$\frac{dk}{d\bar{\eta}} = \frac{\partial \omega^{System A}}{\partial \bar{\eta}}}{V_+ - \frac{\partial \omega^{System A}}{\partial k}}, \tag{46}$$

for the wavenumber at the trailing edge, together with the boundary condition $k = 0$ at $\eta = \eta_+$ to match with the solitary wave edge of the undular bore.^{2,35} As stated above, the Riemann invariant on the characteristic C_- of the non-dispersive equations is conserved through the undular bore. Hence, the Riemann invariant (39) gives

$$\bar{u} = 2\left(\sqrt{1 + \bar{\eta}} - \sqrt{1 + \eta_+}\right), \tag{47}$$

as $\eta = \eta_+$ and $u = 0$ ahead of the bore, which determines the mean velocity \bar{u} in the dispersion relation (45). In addition, this expression for \bar{u} gives that the characteristic velocity V_+ for the Riemann invariant (38) in the differential equation (46) becomes

$$V_+ = \bar{u} + \sqrt{1 + \bar{\eta}} = 3\sqrt{1 + \bar{\eta}} - 2\sqrt{1 + \eta_+}. \tag{48}$$

Using these results and the dispersion relation (45), the compatibility condition (46) becomes

$$\frac{dk}{d\bar{\eta}} = \frac{\frac{\partial \omega^{System A}}{\partial \bar{\eta}}}{V_+ - \frac{\partial \omega^{System A}}{\partial k}} = \frac{k}{2(1 + \bar{\eta})} \frac{2\sqrt{1 - \frac{1}{3}k^2} + 1 - \frac{1}{3}k^2}{\sqrt{1 - \frac{1}{3}k^2} - 1 + \frac{2}{3}k^2}, \tag{49}$$

which determines the position of the trailing edge of the bore. This equation is solved with the boundary condition $k = 0$ at $\bar{\eta} = \eta_+$ to match with the solitary wave edge of the bore.

The differential equation (49) can be solved using the substitution $\sigma^2 = 1 - k^2/3$, which results in

$$\frac{d\sigma}{d\bar{\eta}} = -\frac{1}{2(1 + \bar{\eta})} \frac{(1 + \sigma)(2 + \sigma)}{2\sigma + 1}. \tag{50}$$

Integrating, we find

$$\frac{(2 + \sigma)^3}{1 + \sigma} = \frac{A}{\sqrt{1 + \bar{\eta}}}, \tag{51}$$

where A is a constant of integration. This constant of integration can be found by matching with the leading, solitary wave, edge of the bore, so that $k = 0, \sigma = 1$, at $\bar{\eta} = \eta_+$. Hence

$$A = \frac{27}{2} \sqrt{1 + \eta_+}. \tag{52}$$

The solution for the trailing, linear wave edge of the bore is then completed by noting that it occurs on the intermediate level $\bar{\eta} = \eta_i$. The wavenumber at the trailing edge k_i is then the solution of

$$\frac{\left(2 + \sqrt{1 - \frac{1}{3}k_i^2}\right)^3}{1 + \sqrt{1 - \frac{1}{3}k_i^2}} = \frac{27}{2} \frac{\sqrt{1 + \eta_+}}{\sqrt{1 + \eta_i}}. \tag{53}$$

With the wavenumber at the trailing edge determined, the position of the trailing edge of the bore is determined by the linear group velocity, which from the dispersion relation (45) is

$$c_G^{System A} = 2\left(\sqrt{1 + \eta_i} - \sqrt{1 + \eta_+}\right) + \left[(1 + \eta_i)\left(1 - \frac{1}{3}k_i^2\right)\right]^{1/2} - \frac{1}{3} \frac{k_i^2 \sqrt{1 + \eta_i}}{\sqrt{1 - \frac{1}{3}k_i^2}}. \tag{54}$$

The determination of the solitary wave edge of the undular bore proceeds in a similar manner to the linear wave edge. The wavenumber k and the frequency ω are replaced by a “conjugate” wavenumber \tilde{k} and “conjugate” frequency $\tilde{\omega}$ defined by $\tilde{\omega}^{System A} = -i\omega^{System A}(\bar{u}, \bar{\eta}, ik)$.^{2,35} Equation (46) for the trailing edge of the undular bore then becomes

$$\frac{d\tilde{k}}{d\bar{\eta}} = \frac{\frac{\partial \tilde{\omega}^{System A}}{\partial \bar{\eta}}}{V_+ - \frac{\partial \tilde{\omega}^{System A}}{\partial \tilde{k}}} = \frac{\tilde{k}}{2(1 + \bar{\eta})} \frac{2\sqrt{1 + \frac{1}{3}\tilde{k}^2} + 1 + \frac{1}{3}\tilde{k}^2}{\sqrt{1 + \frac{1}{3}\tilde{k}^2} - 1 - \frac{2}{3}\tilde{k}^2}, \tag{55}$$

for the leading, solitary wave edge. This ordinary differential equation can be solved in a similar manner to the linear wave edge using the change of variable $\tilde{\sigma} = (1 + \tilde{k}^2/3)^{1/2}$ with the boundary condition $\tilde{k} = 0$ at $\bar{\eta} = \eta_i$ to match with the linear wave edge on the intermediate level η_i . The details will not be given, but the final solution for the conjugate wavenumber at the solitary wave edge of the bore \tilde{k}_+ is the solution of

$$\frac{27}{2} \frac{\sqrt{1 + \eta_i}}{\sqrt{1 + \eta_+}} = \frac{\left(2 + \sqrt{1 + \frac{1}{3}\tilde{k}_+^2}\right)^3}{1 + \sqrt{1 + \frac{1}{3}\tilde{k}_+^2}}. \tag{56}$$

The position of the leading edge of the bore is determined by the solitary wave velocity $s_+ = \tilde{\omega}^{System A}/\tilde{k}$, giving

$$s_+ = \left[(1 + \eta_+)\left(1 + \frac{1}{3}\tilde{k}_+^2\right)\right]^{1/2}, \tag{57}$$

on setting $\bar{u} = u_+ = 0$. In addition, using the amplitude–velocity relation (33) for the standard Boussinesq system, the amplitude of the lead solitary wave of the undular bore is

$$a_+ = (1 + \eta_+)\left(1 + \frac{1}{3}\tilde{k}_+^2\right) - 1. \tag{58}$$

The leading and trailing edges of the bore for the standard Boussinesq system have now been determined.

The dispersive shock fitting method can be applied to the other Boussinesq systems in a similar manner. The details of the application of the method to these other systems will then not be given, with just the final result stated. While the leading and trailing edges can be explicitly determined for the standard Boussinesq system (27) and the Boussinesq–Hamiltonian system (28), the differential equation (46) cannot be solved for the Whitham–Boussinesq systems (29) and (30). In these latter cases, these ordinary differential equations will be integrated numerically.

B. System B: Boussinesq–Hamiltonian system

The linear dispersion relation for the Boussinesq–Hamiltonian system (28) is

$$\omega^{System B} = \bar{u}k + k\left[1 + \bar{\eta} - \frac{1}{3}k^2\right]^{1/2}. \tag{59}$$

With this dispersion relation, the differential equation (46) can be solved with the boundary condition $k = 0$ at $\bar{\eta} = \eta_+$ to yield the wavenumber k_i of the trailing edge of the bore as

$$k_i^2 = 3(1 + \eta_i) \left[1 - \left(\frac{2\sqrt{1 + \eta_+} - 1}{\sqrt{1 + \eta_i}} \right)^2 \right], \tag{60}$$

so that its position is determined by the group velocity,

$$c_G^{System B} = 2 \left(\sqrt{1 + \eta_i} - \sqrt{1 + \eta_+} \right) + \sqrt{1 + \eta_i} - \frac{1}{3} k_i^2 - \frac{k_i^2}{3\sqrt{1 + \eta_i} - \frac{1}{3} k_i^2}. \tag{61}$$

The differential equation (55) for the leading edge of the undular bore can be solved to give

$$\tilde{k}_+^2 = 3(1 + \eta_+) \left[\left(\frac{2\sqrt{1 + \eta_i} - 1}{\sqrt{1 + \eta_+}} \right)^2 - 1 \right], \tag{62}$$

for the leading edge conjugate wavenumber, on using the boundary condition $k = 0$ at $\bar{\eta} = \eta_i$, and

$$s_+ = \left[1 + \eta_+ + \frac{1}{3} \tilde{k}_+^2 \right]^{1/2}, \tag{63}$$

for the velocity of the leading edge of the undular bore. The amplitude-velocity relation (35) for the Boussinesq-Hamiltonian solitary wave gives that the amplitude of the leading edge of the undular bore is

$$a_+ = 2 \left[1 + \eta_+ + \frac{1}{3} \tilde{k}_+^2 \right]^{1/2} - 2. \tag{64}$$

C. System C: Full-dispersion shallow water equations

The dispersion relation for the Whitham-Boussinesq system (29) is, by construction,

$$\omega^{System C} = \bar{u}k + \sqrt{(1 + \bar{\eta})k \tanh k}. \tag{65}$$

With this dispersion relation, Eq. (46) for the linear trailing edge is

$$\frac{dk}{d\bar{\eta}} = \frac{\sqrt{k \tanh k}}{1 + \bar{\eta}} \frac{k + \frac{1}{2} \sqrt{k \tanh k}}{\sqrt{k \tanh k} - \frac{1}{2} \tanh k - \frac{1}{2} k \operatorname{sech}^2 k}. \tag{66}$$

Unlike for the previous Boussinesq systems, the solution of this differential equation cannot be found and it has to be integrated numerically with the boundary condition $k = 0$ at $\bar{\eta} = \eta_+$. In a similar fashion, the conjugate form of the dispersion relation (65) can be used in the dispersive shock fitting equation (55) to give

$$\frac{d\tilde{k}}{d\bar{\eta}} = \frac{\sqrt{\tilde{k} \tan \tilde{k}}}{1 + \bar{\eta}} \frac{\tilde{k} + \frac{1}{2} \sqrt{\tilde{k} \tan \tilde{k}}}{\sqrt{\tilde{k} \tan \tilde{k}} - \frac{1}{2} \tan \tilde{k} - \frac{1}{2} \tilde{k} \operatorname{sec}^2 \tilde{k}}, \tag{67}$$

which determines the leading edge of the undular bore, together with the boundary condition $\tilde{k} = 0$ at $\bar{\eta} = \eta_i$. Again, this differential equation is solved numerically. The velocity of the leading edge of the undular bore is then $s_+ = \tilde{\omega}_+^{System C} / \tilde{k}_+$. While the velocity of the

leading edge of the undular bore is determined by the dispersive shock fitting method, the amplitude is not in the absence of the amplitude-velocity relation for the Whitham-Boussinesq solitary wave.

D. System D: Whitham-Boussinesq-Hamiltonian system

The dispersion relation for the Whitham-Boussinesq-Hamiltonian system (30) is

$$\omega^{System D} = \bar{u}k + k \left[\frac{\tanh k}{k} + \bar{\eta} \right]^{1/2}. \tag{68}$$

As for the previous Whitham-Boussinesq equation, the differential equation

$$\frac{dk}{d\bar{\eta}} = \frac{k}{\sqrt{1 + \bar{\eta}}} \frac{\sqrt{\frac{\tanh k}{k} + \bar{\eta}} + \frac{1}{2} \sqrt{1 + \bar{\eta}}}{\sqrt{1 + \bar{\eta}} \sqrt{\frac{\tanh k}{k} + \bar{\eta} - \bar{\eta}} - \frac{1}{2} \frac{\tanh k}{k} - \frac{1}{2} \operatorname{sech}^2 k}, \tag{69}$$

for the trailing edge of the bore can only be solved numerically with the boundary condition $k = 0$ at $\bar{\eta} = \eta_+$. Similarly, the equation

$$\frac{d\tilde{k}}{d\bar{\eta}} = \frac{\tilde{k}}{\sqrt{1 + \bar{\eta}}} \frac{\sqrt{\frac{\tan \tilde{k}}{\tilde{k}} + \bar{\eta}} + \frac{1}{2} \sqrt{1 + \bar{\eta}}}{\sqrt{1 + \bar{\eta}} \sqrt{\frac{\tan \tilde{k}}{\tilde{k}} + \bar{\eta} - \bar{\eta}} - \frac{1}{2} \frac{\tan \tilde{k}}{\tilde{k}} - \frac{1}{2} \operatorname{sec}^2 \tilde{k}}, \tag{70}$$

for the leading edge of the undular bore, together with the boundary condition $\tilde{k} = 0$ at $\bar{\eta} = \eta_i$ is solved numerically. Again, the velocity of the leading edge of the undular bore is $s_+ = \tilde{\omega}_+^{System D} / \tilde{k}_+$, but in the absence of the amplitude-velocity relation for the solitary wave solution, the amplitude of the leading edge is not determined. For the amplitude comparisons of Sec. V, the amplitude of the leading edge of the bore is taken from numerical solutions of Systems C and D.

IV. NUMERICAL METHODS

The numerical solutions of the water wave equations (2)–(5) were found using the Hamiltonian formulation (19) and (20) based on a pseudospectral method.⁵⁶ There are many examples of the application of such methods to solve the water wave equations based on various extensions of these pseudospectral methods.^{57,58} Using the formulation of Guyenne,⁵⁸ we write the Hamiltonian equations (19) and (20) as

$$\mathbf{v}_t = \mathcal{L}\mathbf{v} + \mathcal{N}\mathbf{v}, \text{ where } \mathcal{L} = \begin{pmatrix} 0 & G_0 \\ -g & 0 \end{pmatrix}, \mathcal{N} = \begin{pmatrix} (G - G_0)\xi \\ -\frac{[\xi_x^2 - (G\xi)^2 - 2\xi_x \eta_x G\xi]}{2(1 + \eta_x^2)} \end{pmatrix}, \tag{71}$$

and $\mathbf{v} = (\eta, \xi)^T$.⁵⁸ The system (71) is solved using a split step method where the linear and nonlinear components are solved separately,

$$\mathbf{v}_t = \mathcal{L}\mathbf{v}, \quad \mathbf{v}_t = \mathcal{N}\mathbf{v}. \tag{72}$$

The second-order Strang splitting split step method

$$\mathbf{v}^{n+1} = \mathcal{N}_{\frac{\Delta t}{2}} \mathcal{L}_{\Delta t} \mathcal{N}_{\frac{\Delta t}{2}} \mathbf{v}^n \tag{73}$$

is then used for each time step Δt . The nonlinear equation, the second of (72), is first solved using a half time step, followed by the linear equation, the first of (72), using a full time step, then the nonlinear equation again using a half time step. The linear system itself is solved in Fourier space using the integrating factor method^{59,60} to enhance stability of the scheme for the high-frequency modes, while the nonlinear system is solved using the second-order Runge–Kutta method. Both the Strang split step method and the second-order Runge–Kutta method are second-order accurate in time, giving a $O(\Delta t^2)$ error for the full time evolution. For the nonlinear equation, the operator G and derivative terms are calculated in Fourier space. It was found that three terms in the series (13), up to G_2 , provide sufficient accuracy for this and that adding extra terms made no difference to the solution to the accuracy required here. While the integrating factor method suppresses instability due to high-frequency modes, it was found necessary to further suppress such instability when integrating to the long times required to obtain steady undular bore parameters to compare with solutions of the various Boussinesq systems. This was performed by using the smoothing and filtering techniques suggested by Craig and Sulem⁵⁷ and Guyenne and Nicholls.⁶¹

The numerical calculations of this work were performed with $n = 2^{15}$ Fourier modes, which gives enough accuracy to successfully capture the numerical solution up to the largest initial jumps, with a time step of $dt = 0.01$. To ensure stability of the numerical solution of the water wave equations, we applied a low pass filter. It was found that for $n = 2^{15}$ filtering the higher modes corresponding to wavenumbers lying in the band $[\frac{n}{8}, \frac{n}{2}]$ was adequate to suppress numerical instability, particularly for higher initial jumps. The effect of filtering on the bore solution of the water wave equations was tested by altering the bandwidth. Varying the bandwidth around that used here showed no visible variation in the final bore solution. The major effect of too much filtering was on the trailing edge of the bore as the waves there are of the highest frequency and lowest amplitude. It was found that too much filtering kills the linear wave edge of the bore. The filtering used here showed a good compromise between the high Fourier resolution, $n = 2^{15}$, stable solutions for long time periods, and minimal effect on the resulting solution. For the numerical solutions of the water wave equations, the domain lengths 10 000 or 11 000 were used, depending on the final time chosen for the solution. For the numerical solutions of the present work, the level ahead $\eta_+ = 0$ was used. A non-zero level ahead just involves a rescaling of the equations through an alteration of the undisturbed depth h_0 , which was used to nondimensionalize the water wave equations (2)–(5), to be the total depth ahead of the step.

The smoothing of the initial condition alters the DSW’s oscillatory structure in the neighborhood of the DSW harmonic edge. The initial condition (31) smoothed using hyperbolic tangents is

$$\eta(x, 0) = \eta_+ - \frac{1}{2}(\eta_- - \eta_+) \left[\tanh \frac{x}{W} - \tanh \frac{x - x_-}{W} \right]. \tag{74}$$

This smoothed initial condition has a “top hat” shape with the “brim” level η_+ and the “crown” level η_- . This top hat shape was used for the numerical solution to ensure periodicity in the computational domain for the Fourier solution. The jump across the initial condition is denoted by $\Delta = \eta_- - \eta_+$. If x_- is chosen so that $x_- \ll 0$, then the

smoothed step (74) approximates the initial condition (31) as long as waves generated at $x = 0$ do not reach the step down. It was found that there was some change in the solution as the smoothing width W varied from 10 to 5, mostly at the trailing, linear wave edge of the bore with the leading edge amplitude changing by only 0.2%. Furthermore, as W decreased from 5 to 2, there was no change in the leading edge of the bore and negligible change at the trailing edge which was below the graphical accuracy of the figures shown in Sec. V. This dependence of the bore solution on the smoothing of the initial condition, particularly at the trailing, harmonic edge, is a general property of bores and has been studied and documented for the KdV equation.⁶² For the numerical solutions of Systems A and B and the water wave equations, the smoothing width $W = 2$ was chosen and for Systems C and D, $W = 1$ was chosen. The smaller value of the smoothing width was possible for Systems C and D, as the linear phase velocity is bounded due to $\tanh k$, so that the numerical schemes have better stability.

Figure 2 displays the dependence of the bore solution on the strength of the smoothing width W of the numerical initial condition (74), for $W = 10, 2, 5/3$, for the initial jump $\Delta = 0.28$. It can be seen that the large smoothing width $W = 10$ gives a greatly truncated trailing edge in comparison with the sharper initial conditions with $W = 2$ and $W = 5/3$. In addition, the solutions for $W = 2$ and $W = 5/3$ are identical to graphical accuracy, which gives confidence in the choice $W = 2$ for the water wave solutions of the present work.

In addition, the Boussinesq systems (27) and (28) and the Whitham–Boussinesq systems (29) and (30) were solved numerically using the pseudospectral method of Fornberg and Whitham,⁵⁶ as extended through the use of integrating factors to suppress high-frequency instabilities.^{59,60} These pseudospectral methods use the fast Fourier transform (FFT) to calculate the spatial derivatives, with the solution propagated forward in time using the second-order Runge–Kutta scheme and Strang splitting, which is also second order. Pseudospectral methods are particularly suitable for the Whitham–Boussinesq systems as the dispersion for these systems is given by Fourier integrals. The initial condition (31) was smoothed

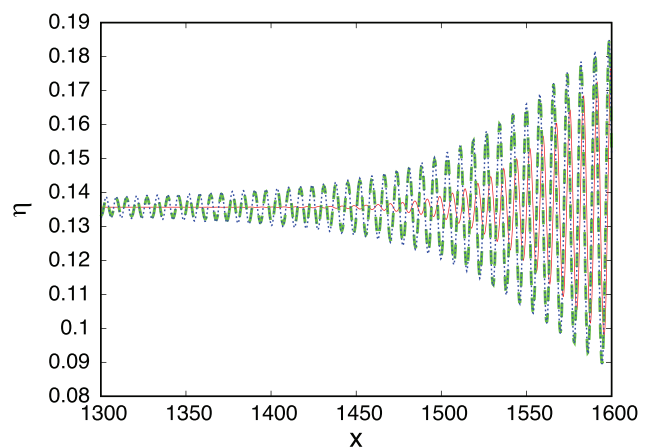


FIG. 2. Trailing edge of the water wave bore at $t = 1700$ for the jump $\Delta = 0.28$ for the smoothing widths $W = 10, 2, 5/3$ of the numerical approximation (74) of the initial condition (31). Red (full) line: trailing edge for $W = 10$; green (dashed) line: trailing edge for $W = 2$; and blue (dotted) line: trailing edge for $W = 5/3$.

using (74) for the numerical solutions of the four Boussinesq and Whitham–Boussinesq systems. It was found that the numerical solution of the Whitham–Boussinesq equations was stable for a smoothing width $W=1$, while for stability the numerical solution of the water wave equations required larger smoothing widths between 2 and 10, with $W=2$ chosen, as stated above. For Systems A, C, and D $n = 2^{16}$ Fourier modes were used with a time step $dt = 0.005$, while for System B $n = 2^{15}$ Fourier modes were used with a time step $dt = 0.01$. Finally, the ordinary differential equations (66), (67) and (69), (70) for the trailing and leading edges of the undular bore for Systems C and D, respectively, were solved using the second-order Runge–Kutta method.

V. COMPARISON OF FULL WATER WAVE THEORY AND WHITHAM–BOUSSINESQ SYSTEMS

Figure 3 shows comparisons for the properties, the lead solitary wave velocity s_+ and amplitude a_+ , of the lead (solitary) wave of the undular bore as given by the full water wave equations (2)–(5), the standard Boussinesq system (27), the Hamiltonian Boussinesq system (28), the Whitham–Boussinesq equation (29), and the Whitham–Boussinesq–Hamiltonian system (30) as the initial jump height $\Delta = \eta_- - \eta_+$ varies until the onset of Benjamin–Feir instability around $\Delta = 0.3$. The issue of unstable bore evolution will be discussed later. The lead wave velocities of the bore for the four Boussinesq systems are given by the dispersive shock wave solutions of Sec. III. As the amplitude–velocity relations for the solitary wave solutions of the Boussinesq equations (27) and (28) are known, see Eqs. (33) and (35), the amplitudes of the lead wave of the bores for the standard Boussinesq system (27) and the Hamiltonian–Boussinesq system (28) are determined by the dispersive shock fitting method, given by (58) and (64), respectively. As the amplitude–velocity relations of the solitary wave for the Whitham–Boussinesq systems (29) and (30) are not known, the amplitudes of the lead wave of the bores for these systems were determined from numerical solutions of the Whitham–Boussinesq systems. In this, and subsequent comparisons, solutions of the Boussinesq and Whitham–Boussinesq systems are color coded, solutions of System A

are denoted by pink (dotted-dashed) lines, solutions of System B by blue (dotted) lines, solutions of System C by red (full) lines, and solutions of System D by green (dashed) lines. The differences in the properties of the lead wave of the bore as given by the Boussinesq systems and the water wave equations are small, until near the onset of instability. The dispersive shock fitting method gives the leading and trailing edges of the bore when these reach their steady values. It was found that the numerical bore solution of the water wave equations took an unrealistic amount of time to reach a steady state, of the order of $t = 20\,000$, as will be discussed below. Hence, to obtain valid comparisons between predictions of the dispersive shock wave fitting method and numerical solutions of the water wave equations, the steady amplitude and velocity of the lead wave of the water wave bore were estimated using extrapolation. It was found that the exponential function

$$\kappa - \beta e^{-\gamma(t-t_0)} \tag{75}$$

gave a good fit to the numerical amplitude and velocity for t_0 chosen large enough so that the start-up transients involved in the formation of the bore have died down. The values of the fitting parameters κ , β and γ were determined from the numerical amplitude and velocity data using a Matlab fitting routine that creates a fit to the velocity and amplitude data with the model specified by (75) and returns fitted parameter values, as well as estimators of confidence intervals. The data were also reprocessed by applying smoothing to reduce the small noise within the velocity and amplitude data. It was found that suitable values of t_0 were from 1500 to 1550, with the fitted parameter values weakly dependent on t_0 in this range. The steady lead wave bore parameters are then given by κ . With this fitted extrapolation function, the time needed for the amplitude and velocity to reach to within 0.01% of the steady state value κ can be estimated, noting that this level of accuracy was needed to show the differences between the four Boussinesq systems and solutions of the water wave equations for the lead wave velocity to graphical accuracy. This time depends on the value of Δ , but was found to vary between 15 000 and 49 000, with the higher values unrealistic for the numerical solution. It should be pointed out that for the fitting procedure, there is a compromise—

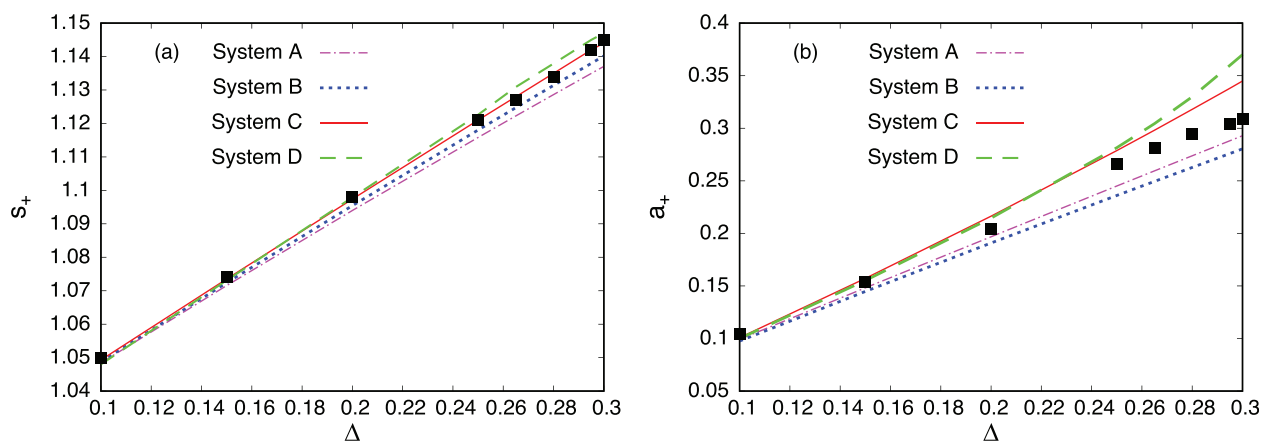


FIG. 3. Comparisons between properties of the lead wave of the undular bore as given by the Boussinesq systems A and B, the Whitham–Boussinesq systems C and D, and the water wave equations. Pink (dotted-dashed) line: solution of standard Boussinesq system (27); blue (dotted) line: solution of Hamiltonian Boussinesq system (28); red (full) line: solution of Whitham–Boussinesq equation (29); and green (dashed) line: solution of Whitham–Boussinesq–Hamiltonian system (30); solution of water wave equations (2)–(5): black squares. (a) Lead wave velocity s_+ and (b) lead wave amplitude a_+ . Here, $\eta_+ = 0$.

since the closer the start of the fitting interval is to the final time, the better the results should be. However, the fitting interval needs to be a minimum length in order to obtain robust results. It was verified that varying the length of the fitting interval around the final length used gave no visible variation in the final parameters.

Figure 3(a) shows that there is excellent agreement between solutions of the Whitham–Boussinesq systems and numerical solutions of the water wave equations for the velocity of the leading edge of the bore, with the velocity as given by Systems A and B being somewhat less than the water wave velocity, the maximum difference for System A being 0.7% and for System B 0.4%. The water wave lead velocity is slightly closer to that given by System C for the larger jump heights until near $\Delta = 0.3$ for which the velocity predicted by System D is closer. Overall, the differences between the predictions of System C and D are small, with a maximum difference from the water wave lead velocity of 0.1% for System C and 0.2% for System D. The comparison starts at the jump height $\Delta = 0.1$ as below this the Boussinesq systems, Whitham–Boussinesq systems and water wave equations give identical results to graphical accuracy. It can be seen that the differences in the lead wave velocities as given by the four Boussinesq systems and the water wave equations are not large, due to the lead wave amplitude not being large before the onset of instability, as seen from Fig. 3(b). An important conclusion is that the Whitham–Boussinesq systems are sufficient to give essentially the same leading edge velocity as the water wave equations. Given the additional complexity in solving and analyzing the water wave equations compared with the KdV-like Whitham–Boussinesq systems, this shows that in this regard the Whitham–Boussinesq systems are sufficient.

Figure 3(b) shows a similar comparison for the amplitude of the leading edge of the bore. The agreement between the solutions of the Boussinesq systems and the solution of the water wave equations is not as good as for the leading edge velocity. This is typical for bore solutions of nonlinear dispersive wave equations, which typically show better agreement for the leading edge velocity than the leading edge amplitude.² The comparison shows that the amplitude of the bore as given by the water wave equations lies between the amplitude as given by the Boussinesq and Whitham–Boussinesq systems, but is closer to the amplitude given by the Whitham–Boussinesq systems. The amplitude as given by the Whitham–Boussinesq systems grows much more rapidly as the jump height Δ increases toward the onset of instability around $\Delta = 0.3$, with the difference growing from 5% at $\Delta = 0.25$ to 12% at $\Delta = 0.30$ and from 6% at $\Delta = 0.25$ to 20% at $\Delta = 0.3$ for Systems C and D, respectively. This growing disagreement is tied to the growth of the instability of the bore solution of the Whitham–Boussinesq systems as $\Delta = 0.3$ is approached, as will be discussed in detail below.

Figure 4 shows comparisons between solutions of the two Boussinesq systems (27) and (28) and the two Whitham–Boussinesq systems (29) and (30) with numerical solutions of the water wave equations (2)–(5) for the jump $\Delta = 0.15$ with the bore moving into undisturbed depth. For this jump height, Fig. 3 shows that there is little difference in the amplitude and velocity of the lead wave of the undular bore between Systems A to D and the water wave equations. The greatest difference is in the lead wave amplitude, with the water wave amplitude being between those of Systems A and B and Systems C and D, but closer to the latter amplitudes. These general results are confirmed by the solutions at $t = 1700$ displayed in Fig. 4. It should be

noted that at $t = 1700$ neither the lead wave amplitude nor the lead wave velocity have reached the steady state values displayed in Fig. 3, as discussed at the beginning of this section. As the initial jump creating the undular bore is low, there is little difference in the solutions of Systems A to D. There is some difference in the envelope of the undular bores as given by these systems and the full water wave equations, but the main difference between the water wave bore and the Boussinesq and Whitham–Boussinesq bores is a phase difference, with the water wave bore behind these weakly nonlinear bores. To leading order Whitham modulation theory does not determine the modulated phase of the wavetrain.² The determination of this modulated phase requires the extension of Whitham modulation theory to next order, which is non-trivial.^{63,64} The position of the trailing edge of the undular bore is given by (54), (61), (66), and (69) for Systems A to D, respectively. The thick blue line in the figures shows the intermediate level u_i given by (43). This line terminates at the trailing edge position as given by the Boussinesq and Whitham–Boussinesq systems. The final observation from Fig. 4 is that all four weakly nonlinear systems give a good prediction for the location of the trailing edge of the water wave bore. There is no distinct location for the trailing edge as there is for the leading edge since there is an extended wavetrain propagating upstream, so its location is subjective. The trailing edge group velocity for Systems A and B is slightly lower than that for Systems C and D, so that the trailing edge position for Systems A and B corresponds to lower amplitude waves of the water wave bore. An approximation to the trailing edge of an undular bore is to extrapolate the envelope of the waves at the rear of the bore down to the intermediate level u_i . If this is done for the water wave bore of Fig. 4, then this position lies between those predicted by Systems A, B and Systems C, D.

Figure 3 shows that the leading solitary wave of the undular bore is well predicted by the two Whitham–Boussinesq systems (29) and (30). The original motivation for the introduction of Whitham-type equations was that the inclusion of the full linear dispersion relation introduces short wave effects which are not present in equations on which they are based,¹ for instance, the Boussinesq systems (27) and (28). One of these is modulational instability (MI), also termed Benjamin–Feir instability.¹ For jump heights Δ above 0.3, the undular bore solutions of the two Whitham–Boussinesq systems and the water wave equations develop instability, which starts in the interior of the bore. It should be noted that careful tests were made by varying the time step and the number of modes used for the computational interval to verify that these instabilities were not numerical. Figure 5 illustrates the development of the instability above the jump $\Delta = 0.3$ for Systems C and D and the water wave equations. The thick blue lines in Fig. 5 show the intermediate level η_i (43). As for Fig. 4, this line terminates at the trailing linear edge of the bore as determined by (66) and (69). Figures 5(a) and 5(b) show the development of the instability for System C as the jump height increases. Below $\Delta = 0.3025$, numerical solutions do not show any sign of instability up to $t = 2000$. Figure 5(a) shows that for the jump $\Delta = 0.303$ instability first develops in the interior of the bore, as was found for the original Whitham equation based on the KdV equation.⁶⁵ The wavenumber in this unstable region is around $k = 0.90$, which is comparable with the wavenumber $k = 0.96$ of the initial unstable region of the bore for the Whitham equation.⁶⁵ The wavenumber instability threshold for gravity water waves is $k = 1.36^1$ (since the depth h_0 has been normalized to 1). However, this result is for the stability of a gravity wave Stokes

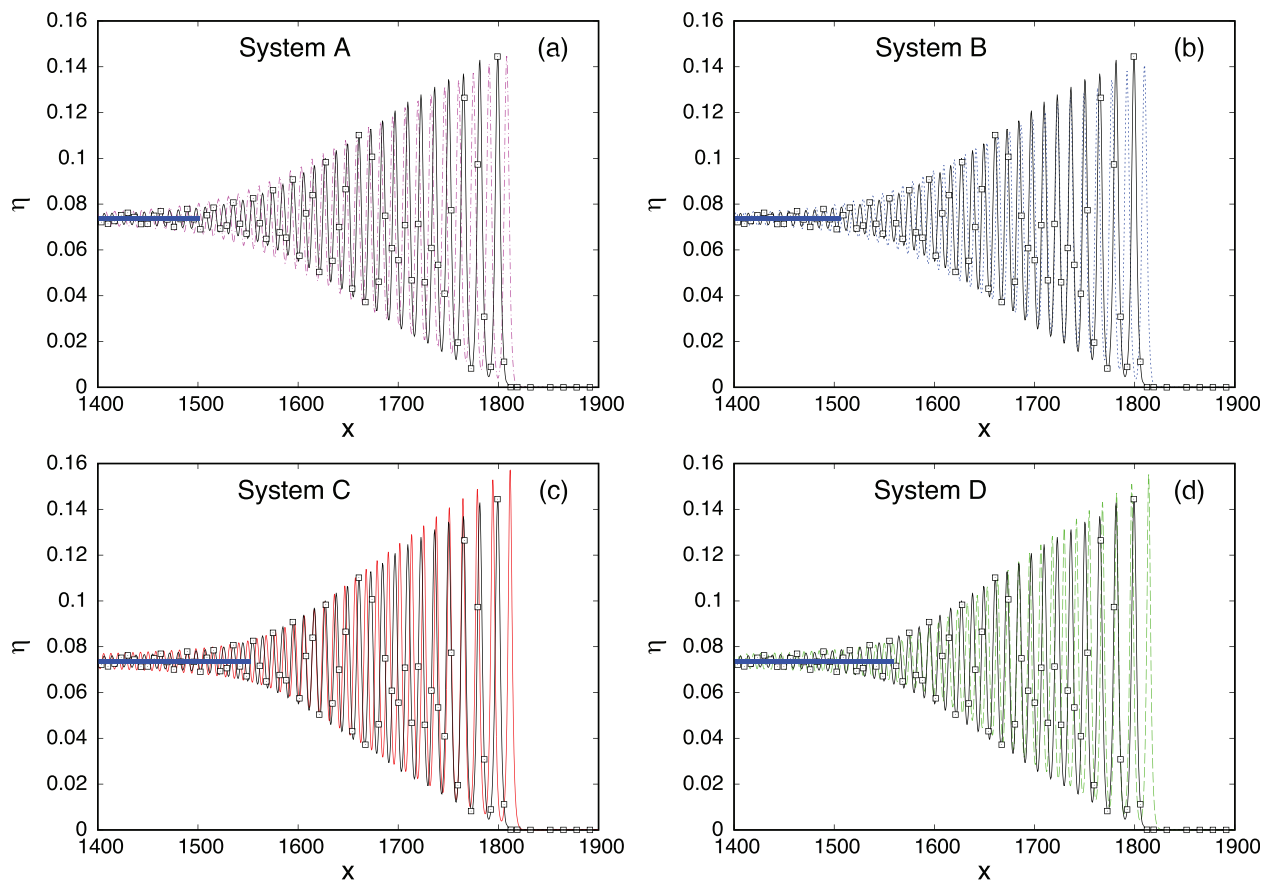


FIG. 4. Stable bore solutions of Boussinesq systems A (27) and B (28), the Whitham–Boussinesq systems C (29) and D (30) and the water wave equations (2)–(5) for $\Delta = 0.15$ at $t = 1700$. (a) System A: pink (dotted-dashed) line; water wave equations: black (full) line with squares. (b) System B: blue (dotted) line, water wave equations: black (full) line with squares. (c) System C: red (full) line; water wave equations: black (full) line with squares. (d) System D: green (dashed) line; water wave equations: black (solid) line with squares. Intermediate level (43): thick blue line.

wavetrain. The interiors of Whitham–Boussinesq undular bores are far from a Stokes wave, so these wavenumbers are not totally comparable. However, given these restrictions, the instability wavenumbers are in reasonable agreement. The final comment is that modulation theory gives a good prediction for the trailing edge of the bore even though the bore is becoming unstable. Further increase in the step height Δ results in the instability becoming more pronounced, as expected, as illustrated in Fig. 5(b). The intermediate level is well predicted, but there is an extended wavetrain beyond the theoretical trailing edge, as is common for undular bore solutions determined from Whitham modulation equations.²

Figures 5(c) and 5(d) illustrate a similar development of the instability, but for System D. The solution of Fig. 5(c) shows the development of the instability for a step height, $\Delta = 0.315$, which is just above the threshold for the onset of instability. It can be seen that there is a modulation of the bore envelope, in contrast to the smooth envelope of Fig. 4(d). The wavenumber of this envelope oscillation is around $k = 0.87$, which is very close to the instability wavenumber of Fig. 5(a) for System C and in basic accord with the Benjamin–Feir instability threshold. There is then a distinct difference between the predictions

of the Whitham–Boussinesq equations of Systems C and D. The instability for System C develops in a finite region interior to the bore, as for the Whitham equation,⁶⁵ but the instability for System D develops as a modulation over the entire bore. Figure 5(d) illustrates a fully unstable bore for the slightly higher step $\Delta = 0.32$. The instability is stronger than that for System C in Fig. 5(b). The bore breaks up with a series of solitary-like waves being shed ahead. The amplitudes of the waves of the bore itself are more uniform than in a stable bore, as for the unstable bore of System C in Fig. 5(c), and the actual amplitude distribution is random, as expected. This overall structure of the unstable bores for Systems C and D, the more uniform amplitude distribution than for stable bores and the random nature of individual waves, is common for unstable bores.⁶⁶

Figures 5(e) and 5(f) show the development of instability for the DSW solution of the water wave equations in a similar manner to Systems C and D. Figure 5(e) shows the water wave DSW for the jump $\Delta = 0.36$, which is the jump height for the onset of instability and Fig. 5(f) shows the DSW for $\Delta = 0.37$, which is fully unstable. The water wave DSW for the jump $\Delta = 0.35$ and below shows no instability. The thick blue lines in these figures show the intermediate

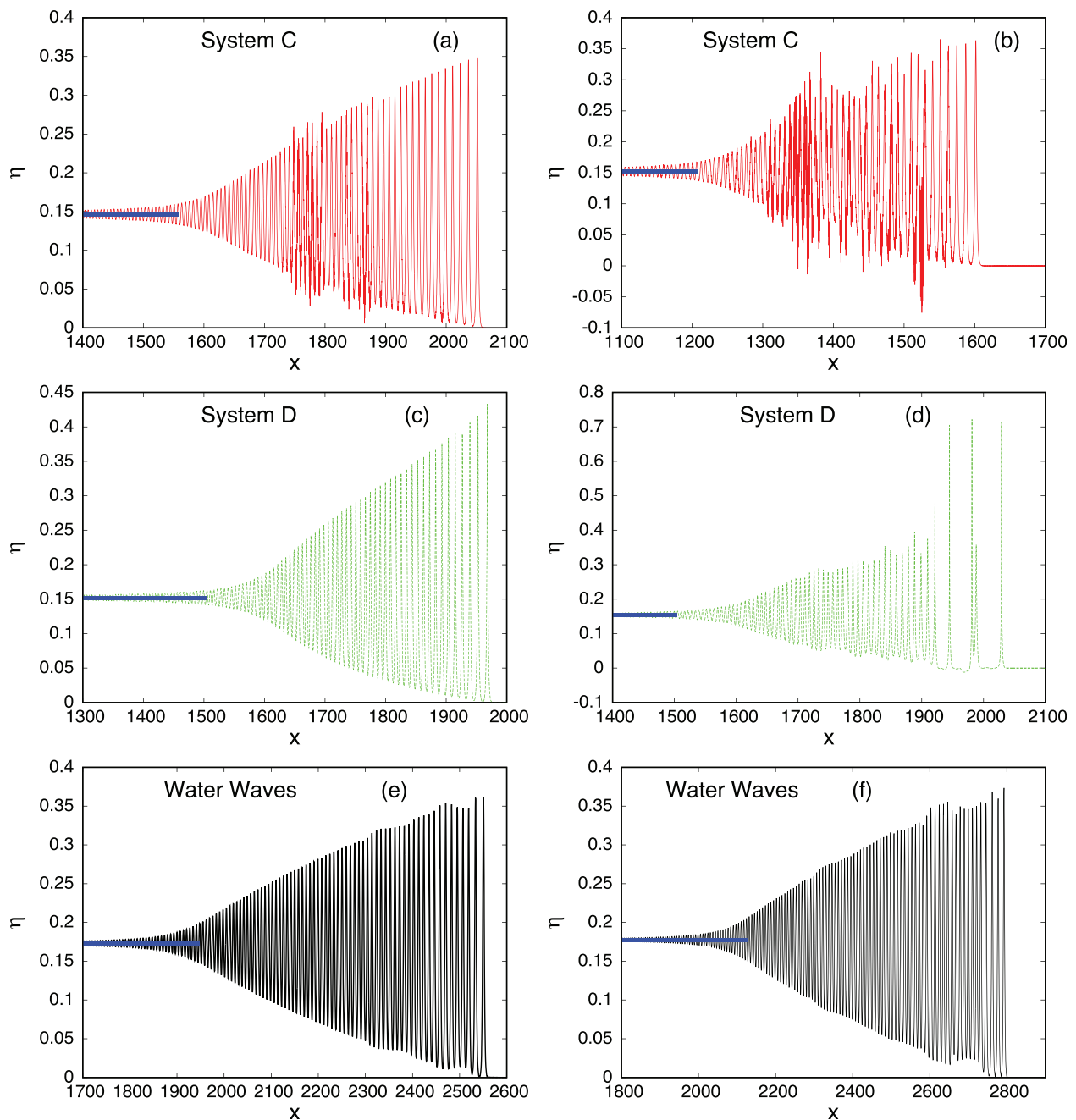


FIG. 5. Solutions of Whitham–Boussinesq systems C (29) and D (30) and the water wave equations (2)–(5). (a) System C: red (full) line at $t = 1800$ for $\Delta = 0.303$, (b) System C: red (full) line at $t = 1400$ for $\Delta = 0.315$, (c) System D: green (dashed) line at $t = 1700$ for $\Delta = 0.315$, (d) System D: green (dashed) line at $t = 1700$ for $\Delta = 0.32$, (e) water wave equations: black (solid) line at $t = 2200$ for $\Delta = 0.36$, and (f) water wave equations: black (solid) line at $t = 2400$ for $\Delta = 0.37$. Intermediate level (43): thick blue line.

level given by (43) with these lines terminating at the trailing edge position (69) of System D. The borderline unstable water wave DSW of Fig. 5(e) shows an overall envelope modulation, which is similar to the borderline unstable DSW for System D shown in Fig. 5(c) and differs from the borderline unstable DSW for System C shown in

Fig. 5(a) for which the instability develops in a restricted region interior to the DSW. The wavenumber of the water wave DSW at the upstream edge of the unstable region near $x = 2250$ is $k = 0.76$, which is not near the Benjamin–Feir threshold of $k = 1.36$ and further from $k = 1.36$ than the unstable Systems C and D DSWs. The upstream

edge of the unstable portion of the DSW starts near its center, which is far from a Stokes wave. System D then gives a better prediction of the initial development of water wave DSW instability than System C. Figure 5(f) shows a fully unstable water wave bore for the initial jump $\Delta = 0.37$. There is a modulation of the bore envelope, which is similar to that of Fig. 5(e), but stronger. The noticeable difference with the fully unstable System D bore of Fig. 5(d) is that there is not the generation of large amplitude solitary waves at the leading edge due to the instability. Overall, System D gives a better prediction of the development of the instability and gives a better prediction of the stability threshold, but both Systems C and D give stability thresholds below that of the water wave equations. This is not unexpected as the Whitham–Boussinesq equations are being pushed beyond their region of expected validity.

VI. CONCLUSIONS

The formation and propagation of surface water wave undular bores have been studied using four Boussinesq systems. Two of these were standard Boussinesq systems for weakly nonlinear long waves, one the standard Boussinesq system¹ and the other the system arising from the Hamiltonian formulation of the water wave equations.⁵¹ The other two Boussinesq systems were Whitham equation^{1,44} extensions of these Boussinesq systems which are still weakly nonlinear, but include full linear water wave dispersion. The undular bore solutions of these four Boussinesq systems were compared with numerical solutions of the full water wave equations. It was found that the two Whitham–Boussinesq systems give improved agreement with solutions of the water wave equations, as expected. The major result found is that the Whitham–Boussinesq systems give near excellent agreement with solutions of the water wave equations for the positions of the leading and trailing edges of the undular bore.

It is found that the Whitham–Boussinesq system C and the Whitham–Boussinesq system D derived from the Hamiltonian formulation of the water wave equations give excellent agreement for the velocities of the leading and trailing edges of the bore, better than those given by solutions of the Boussinesq systems A and B. The agreement for the amplitude of the lead wave of the undular bore is not as good as for the lead wave velocity, but again the bidirectional Whitham systems, Whitham–Boussinesq systems, are in better agreement than the Boussinesq systems. In addition, the Whitham–Boussinesq systems give accurate predictions for the initial surface step height for the onset of modulational instability (MI), noting that this instability does not occur for the original Boussinesq systems. The growing differences between the amplitudes of the bore as given by the Whitham–Boussinesq systems and the full water wave equations as the height of the initial jump which generates the bore increases is linked to the onset of instability since solutions of the Whitham–Boussinesq systems show much greater variations in the amplitudes of the individual waves of the bore in the unstable regime. Above a nondimensional initial step height of 0.3, there is a rapid transition to the unstable regime for bore solutions of the two Whitham–Boussinesq systems and a somewhat slower transition to instability for the bore solution of the full water wave equations. As a summary, it is found that the Whitham–Boussinesq systems give excellent agreement with undular bore solutions of the full water wave equations up until the onset of instability, so much so that they could

be used as an alternative to the full water wave equations, noting that they are much simpler to solve and analyze.

The two Whitham–Boussinesq systems, Systems C and D, give very accurate predictions for the velocity of the leading edge of the undular bore up until the onset of modulational instability. System D is in better agreement with solutions of the water wave equations for $\Delta < 0.22$, while System C is better above this jump height. However, the maximum difference between the lead wave velocity as given by System D and the water wave equations is 0.2%, while the maximum difference for System C is 0.1%, so both systems give very accurate predictions and there is not much between these two Whitham–Boussinesq systems. The amplitude of the lead wave of the undular bore is not as well predicted as the leading and trailing edge velocities by the Whitham–Boussinesq systems. The agreement between the amplitudes given by Systems C and D with the water wave amplitude follows the same general trend as for the lead wave velocity, with System D being better for $\Delta < 0.22$ and System C better above this value. In addition, the Whitham–Boussinesq–Hamiltonian system, System D, gives a good prediction for the initial jump height Δ for the onset of modulational instability of the undular bore, better than that of System C, and for the overall development of this instability. In summary, the Whitham–Boussinesq systems are very accurate models of surface water wave undular bore propagation. Indeed, they can be concluded to provide a very accurate alternative to the full water wave equations for the study of water wave undular bores. This could prove useful as Whitham-type equations are much easier to solve and analyze than the full water wave equations.

ACKNOWLEDGMENTS

R.M.V.-M. was funded by Consejo Nacional de Ciencia y Tecnología (CONACyT), calls, EPE2018(1) and EPE2019(2), Estancias Posdoctorales en el Extranjero Vinculadas a la Consolidación de Grupos de Investigación y Fortalecimiento del Posgrado Nacional Año 2018 y Continuidad en 2019 (Postdoctoral stay abroad granted by the Mexican National Council of Science and Technology to develop a submitted research project, year 2018 and extension in 2019). R.M.V.-M. would also like to thank CONACyT and the collective “Científicas Mexicanas en el Extranjero” for funding her postdoctoral position at the University of Edinburgh.

DATA AVAILABILITY

The data that support the findings of this study are available from the corresponding author upon reasonable request.

REFERENCES

- ¹G. B. Whitham, *Linear and Nonlinear Waves* (John Wiley and Sons, New York, 1974).
- ²G. A. El and M. A. Hoefer, “Dispersive shock waves and modulation theory,” *Phys. D* **333**, 11–65 (2016).
- ³D. R. Christie, “Long nonlinear waves in the lower atmosphere,” *J. Atmos. Sci.* **46**, 1462–1491 (1989).
- ⁴R. H. Clarke, R. K. Smith, and D. G. Reid, “The morning glory of the Gulf of Carpentaria: An atmospheric undular bore,” *Mon. Weather Rev.* **109**, 1726–1750 (1981).
- ⁵V. A. Porter and N. F. Smyth, “Modelling the morning glory of the Gulf of Carpentaria,” *J. Fluid Mech.* **454**, 1–20 (2002).

- ⁶N. F. Smyth and P. E. Holloway, "Hydraulic jump and undular bore formation on a shelf break," *J. Phys. Oceanogr.* **18**, 947–962 (1988).
- ⁷P. G. Baines, *Topographic Effects in Stratified Flows* (Cambridge Monographs on Mechanics, Cambridge, 1995).
- ⁸C. Yuan, R. Grimshaw, and E. Johnson, "The evolution of internal undular bores over a slope in the presence of rotation," *Stud. Appl. Math.* **140**, 465–482 (2018).
- ⁹V. V. Novotryasov, D. V. Stepanov, and I. O. Yaroshchuk, "Observations of internal undular bores on the Japan/East Sea shelf-coastal region," *Ocean Dyn.* **66**, 19–25 (2016).
- ¹⁰T. Talipova, E. Pelinovsky, O. Kurkina, and A. Kurkin, "Numerical modeling of the internal dispersive shock wave in the ocean," *Shock Vib.* **2015**, 875619.
- ¹¹J. G. Esler and J. D. Pearce, "Dispersive dam-break and lock-exchange flows in a two-layer fluid," *J. Fluid Mech.* **667**, 555–585 (2011).
- ¹²S. K. Ivanov and A. M. Kamchatnov, "Formation of dispersive shock waves in evolution of a two-temperature collisionless plasma," *Phys. Fluids* **32**, 126115 (2020).
- ¹³D. R. Scott and D. J. Stevenson, "Magma solitons," *Geophys. Res. Lett.* **11**, 1161–1164, <https://doi.org/10.1029/GL011i011p01161> (1984).
- ¹⁴D. R. Scott and D. J. Stevenson, "Magma ascent by porous flow," *Geophys. Res. Lett.* **91**, 9283–9296, <https://doi.org/10.1029/JB091iB09p09283> (1986).
- ¹⁵N. K. Lowman and M. A. Hofer, "Dispersive shock waves in viscously deformable media," *J. Fluid Mech.* **718**, 524–557 (2013).
- ¹⁶T. R. Marchant and N. F. Smyth, "Approximate solutions for magma propagation from a reservoir," *IMA J. Appl. Math.* **70**, 796–813 (2005).
- ¹⁷C. Barsi, W. Wan, C. Sun, and J. W. Fleischer, "Dispersive shock waves with nonlocal nonlinearity," *Opt. Lett.* **32**, 2930–2932 (2007).
- ¹⁸W. Wan, S. Jia, and J. W. Fleischer, "Dispersive superfluid-like shock waves in nonlinear optics," *Nat. Phys.* **3**, 46–51 (2007).
- ¹⁹G. A. El, A. Gammal, E. G. Khamis, R. A. Kraenkel, and A. M. Kamchatnov, "Theory of optical dispersive shock waves in photorefractive media," *Phys. Rev. A* **76**, 053813 (2007).
- ²⁰M. Conforti, F. Baronio, and S. Trillo, "Resonant radiation shed by dispersive shock waves," *Phys. Rev. A* **89**, 013807 (2014).
- ²¹G. Xu, A. Mussot, A. Kudlinski, S. Trillo, F. Copie, and M. Conforti, "Shock wave generation triggered by a weak background in optical fibres," *Opt. Lett.* **41**, 2656–2659 (2016).
- ²²X. An, T. R. Marchant, and N. F. Smyth, "Optical dispersive shock waves in defocusing colloidal media," *Phys. D* **342**, 45–56 (2017).
- ²³N. F. Smyth, "Dispersive shock waves in nematic liquid crystals," *Phys. D* **333**, 301–309 (2016).
- ²⁴G. A. El and N. F. Smyth, "Radiating dispersive shock waves in non-local optical media," *Proc. R. Soc. London, Ser. A* **472**, 20150633 (2016).
- ²⁵J. Nuño, C. Finot, G. Xu, G. Millot, M. Erkintalo, and J. Fatome, "Vectorial dispersive shock waves in optical fibers," *Commun. Phys.* **2**, 138 (2019).
- ²⁶S. Baqer and N. F. Smyth, "Modulation theory and resonant regimes for dispersive shock waves in nematic liquid crystals," *Phys. D* **403**, 132334 (2020).
- ²⁷C. G. Hooper, P. D. Ruiz, J. M. Huntley, and K. R. Khusnutdinova, "Undular bores generated by fracture," *Phys. Rev. B* (submitted) (2021).
- ²⁸G. A. El, A. M. Kamchatnov, V. V. Khodorovskii, E. S. Annibale, and A. Gammal, "Two-dimensional superionic nonlinear Schrödinger flow past an extended obstacle," *Phys. Rev. E* **80**, 046317 (2009).
- ²⁹P. A. Praveen Janantha, P. Sprenger, M. A. Hofer, and M. Wu, "Observation of self-cavitating envelope dispersive shock waves in yttrium iron garnet thin films," *Phys. Rev. Lett.* **119**, 024101 (2017).
- ³⁰N. K. Lowman and M. A. Hofer, "Fermionic shock waves: Distinguishing dissipative versus dispersive resolutions," *Phys. Rev. A* **88**, 013605 (2013).
- ³¹G. B. Whitham, "A general approach to linear and non-linear dispersive waves using a Lagrangian," *J. Fluid Mech.* **22**, 273–283 (1965).
- ³²G. B. Whitham, "Non-linear dispersive waves," *Proc. R. Soc. London, Ser. A* **283**, 238–261 (1965).
- ³³A. V. Gurevich and L. P. Pitaevskii, "Nonstationary structure of a collisionless shock wave," *Sov. Phys. - JETP* **33**, 291–297 (1974).
- ³⁴H. Flaschka, M. G. Forest, and D. W. McLaughlin, "Multiphase averaging and the inverse spectral solution of the Korteweg-de Vries equation," *Commun. Pure Appl. Math.* **33**, 739–784 (1980).
- ³⁵G. A. El, "Resolution of a shock in hyperbolic systems modified by weak dispersion," *Chaos* **15**, 037103 (2005).
- ³⁶J. W. Miles, "On Hamilton's principle for surface waves," *J. Fluid Mech.* **83**, 153–158 (1977).
- ³⁷A. C. Radder, "An explicit Hamiltonian formulation of surface waves in water of finite depth," *J. Fluid Mech.* **237**, 435–455 (1992).
- ³⁸V. E. Zakharov, "Stability of periodic waves of finite amplitude on the surface of a deep fluid," *J. Appl. Mech. Tech. Phys.* **9**, 190–194 (1968).
- ³⁹P. Aceves-Sánchez, A. A. Minzoni, and P. Panayotaros, "Numerical study of a nonlocal model for water-waves with variable depth," *Wave Motion* **50**, 80–93 (2013).
- ⁴⁰R. M. Vargas-Magaña and P. Panayotaros, "A Whitham-Boussinesq long-wave model for variable topography," *Wave Motion* **65**, 156–174 (2016).
- ⁴¹V. Hur and L. Tao, "Wave breaking in a shallow water model," *SIAM J. Math. Anal.* **50**, 354–380 (2018).
- ⁴²V. Hur and A. K. Pandey, "Modulational instability in a full-dispersion shallow water model," *Stud. Appl. Math.* **142**, 3–47 (2019).
- ⁴³J. D. Carter, "Bidirectional Whitham equations as models of waves on shallow water," *Wave Motion* **82**, 51–61 (2018).
- ⁴⁴G. B. Whitham, "Variational methods and applications to water waves," *Proc. R. Soc. London, Ser. A* **299**, 6–25 (1967).
- ⁴⁵P. I. Naumkin and A. Shishmarev, *Nonlinear Nonlocal Equations in the Theory of Waves*, Translations of Mathematical Monographs (American Mathematical Society, Rhode Island, 1994).
- ⁴⁶A. Constantin and J. Escher, "Wave breaking for nonlinear nonlocal shallow water equations," *Acta Math.* **181**, 229–243 (1998).
- ⁴⁷M. Ehrnström and H. Kalisch, "Traveling waves for the Whitham equation," *Differ. Integr. Equations* **22**, 1193–1210 (2009).
- ⁴⁸M. Ehrnström, M. D. Groves, and E. Wahlén, "On the existence and stability of solitary-wave solutions to a class of evolution equations of Whitham type," *Nonlinearity* **25**, 2903–2936 (2012).
- ⁴⁹M. Ehrnström and E. Wahlén, "On Whitham's conjecture of a highest cusped wave for a nonlocal dispersive equation," *Ann. Inst. Henri Poincaré, Sect. C* **36**, 1603–1637 (2019).
- ⁵⁰V. M. Hur, "Wave breaking in the Whitham equation," *Adv. Math.* **317**, 410–437 (2017).
- ⁵¹W. Craig, P. Guyenne, D. P. Nicholls, and C. Sulem, "Hamiltonian long-wave expansions for water waves over a rough bottom," *Proc. R. Soc. A* **461**(2055), 839–887 (2005).
- ⁵²D. Moldabaye, H. Kalisch, and D. Dutykh, "The Whitham equation as a model for surface water waves," *Phys. D* **309**, 99–107 (2015).
- ⁵³H. Borluk, H. Kalisch, and D. P. Nicholls, "A numerical study of the Whitham equation as a model for steady surface water waves," *J. Comput. Appl. Math.* **296**, 293–302 (2016).
- ⁵⁴T. B. Benjamin, "Instability of periodic wavetrain in nonlinear dispersive systems," *Proc. R. Soc. London, Ser. A* **299**, 59–76 (1967).
- ⁵⁵W. Craig and M. D. Groves, "Hamiltonian long-wave approximations to the water-wave problem," *Wave Motion* **19**, 367–389 (1994).
- ⁵⁶B. Fornberg and G. B. Whitham, "A numerical and theoretical study of certain non-linear wave phenomena," *Philos. Trans. R. Soc., A* **289**, 373–404 (1978).
- ⁵⁷W. Craig and C. Sulem, "Numerical simulation of gravity waves," *J. Comput. Phys.* **108**, 73–83 (1993).
- ⁵⁸P. Guyenne, "A high-order spectral method for nonlinear water waves in the presence of a linear shear current," *Comput. Fluids* **154**, 224–235 (2017).
- ⁵⁹L. N. Trefethen, *Spectral Methods in MATLAB* (SIAM, Philadelphia, 2000).
- ⁶⁰T. F. Chan and T. Kerkhoven, "Fourier methods with extended stability intervals for KdV," *SIAM J. Numer. Anal.* **22**, 441–454 (1985).
- ⁶¹P. Guyenne and D. Nicholls, "Numerical simulation of solitary waves on plane slopes," *Math. Comput. Simul.* **69**, 269–281 (2005).
- ⁶²T. Grava and C. Klein, "Numerical study of a multiscale expansion of the Korteweg-de Vries equation and Painlevé-II equation," *Proc. R. Soc. A* **464**, 733–757 (2008).

- ⁶³R. Haberman, “The modulated phase shift for weakly dissipated nonlinear oscillatory waves of the Korteweg-de Vries type,” *Stud. Appl. Math.* **78**, 73–90 (1988).
- ⁶⁴M. J. Ablowitz, J. T. Cole, and I. Rumanov, “Whitham equations and phase shifts for the Korteweg-de Vries equation,” *Proc. R. Soc. London, Ser. A* **476**, 20200300 (2020).
- ⁶⁵X. An, T. R. Marchant, and N. F. Smyth, “Dispersive shock waves governed by the Whitham equation and their stability,” *Proc. R. Soc. London, Ser. A* **474**, 20180278 (2018).
- ⁶⁶G. A. El, E. G. Khamis, and A. Tovbis, “Dam break problem for the focusing nonlinear Schrödinger equation and the generation of rogue waves,” *Nonlinearity* **29**, 2798–2836 (2016).